THE JOURNAL OF PHYSICAL CHEMISTRY C

ARTICLE

pubs.acs.org/JPCC

Compressional Behavior of Bulk and Nanorod $LiMn_2O_4$ under Nonhydrostatic Stress

Yu Lin,[*,†] Yuan Yang,[‡] Hongwei Ma,[†] Yi Cui,[‡] and Wendy L. Mao[†,§]

[†]Department of Geological and Environmental Sciences and [‡]Department of Materials Science and Engineering, Stanford University, Stanford, California 94305, United States

[§]Photon Science, SLAC National Accelerator Laboratory, Menlo Park, California 94025, United States

ABSTRACT: We studied the effect of pressure on $LiMn_2O_4$ commercial powders and well-characterized nanorods using angle-dispersive synchrotron X-ray diffraction (XRD) in diamond anvil cells and found that spinel $LiMn_2O_4$ is extremely sensitive to deviatoric stress induced by external applied pressure. Under nonhydrostatic conditions, bulk $LiMn_2O_4$ underwent an irreversible phase transformation at pressures as low as 0.4 GPa from a cubic *Fd*-3*m* to tetragonal $I4_1/amd$ structure driven by the Jahn−Teller effect. In contrast, bulk $LiMn_2O_4$ under hydrostatic conditions experienced a reversible structural transformation beginning at approximately 11 GPa. Well-characterized $LiMn_2O_4$ nanorods with an average diameter of 100−150 nm and an average length of 1−2 μm were investigated under the same experimental conditions and showed a similar structural behavior as the bulk material confirming that $LiMn_2O_4$ displays an extremely sensitive structural response to deviatoric stress. Scanning electron microscope (SEM) images of the samples especially the nanorods that were recovered from high pressure demonstrated a link between the changing morphology of the materials and the origin of the phase transition. We also found that nanostructured materials can accommodate more stress compared to their bulk counterparts. Our comparative study of bulk and nanorod $LiMn_2O_4$ improves our understanding of their fundamental structural and mechanical properties, which can provide guidance for applied battery technology. In addition, $LiMn_2O_4$ represents a strongly correlated system, whose structural, electronic, and magnetic properties at high pressure are of broad interest for fundamental chemistry and condensed matter physics.

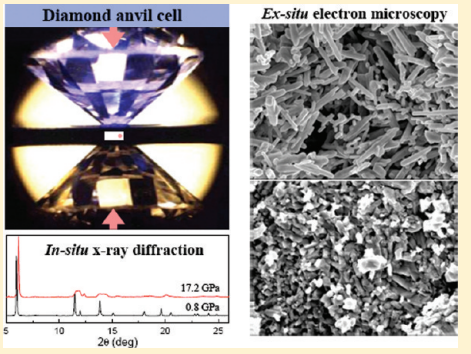

INTRODUCTION

Rechargeable lithium ion batteries have a wide range of applications from portable electronics, power tools, and electric vehicles.[1−4] Nanostructuring battery materials has emerged as an attractive method for further enhancing the battery performance.[5] Spinel $LiMn_2O_4$ has attracted considerable attention as a cathode material due to its high power density, low cost, environmental friendliness, and high abundance.[6−8] The electrochemical activity of $Li_xMn_2O_4$ originates from the redox reaction of Mn^{3+}/Mn^{4+}, which results in two redox plateaus at 4 and 3 V versus Li/Li^+, respectively.[9] At the 4 V plateau ($0 < x < 1$), Mn^{3+} represents less than half of all Mn ions. As a result, the Jahn−Teller distortion of Mn^{3+} ions is not significant and the spinel structure is stable. In contrast, as more lithium ($1 < x < 2$) is inserted into the material, Mn^{3+} ions start to dominate and induce a distorted structure due to internal strain arising from the Jahn−Teller distortion. Such a phase transition significantly deteriorates the cycle life of $LiMn_2O_4$ and the 3 V plateau is not practically usable. Recently, Woodford et al.[10] predicted that even for the 4 V plateau $Li_xMn_2O_4$ particles would experience an internal stress as high as 0.8 GPa at high galvanostatic charging rate, leading to fracture of the electrode particles. In addition, the power rate threshold beyond which fracture events occur decreases with increasing particle size.

Because the electrochemical performance of $LiMn_2O_4$ is strongly influenced by the stresses in the battery environment, to study the pressure-induced phase transitions in $LiMn_2O_4$ can serve as a diagnostic tool to help us better understand and design improved lithium cathode materials. Pressure, a fundamental thermodynamic and clean tuning parameter, can be used to modify the behavior of materials dramatically and has not been fully explored. No consensus has been reached regarding the behavior of $LiMn_2O_4$ under compression, such as the threshold pressure over which the phase transition occurs, and the symmetry as well as the metastability field of the high-pressure phase.

Stoichiometric $LiMn_2O_4$ is a cubic *Fd*-3*m* phase at ambient conditions, and was reported to undergo a first-order phase transition to a tetragonal $I4_1/amd$ structure at 280 K,[11] or to an orthorhombic *Fddd* phase at 290 K with a superstructure unit cell in a more recent study.[12] Previous high-pressure studies found that the structural transition of bulk $LiMn_2O_4$ spinel at room temperature occurs at very modest pressures. The transition pressures for different pressure transmitting media were reported to be below 0.5 GPa[13] and 1.2 GPa[14] in silicon oil, 0.2 GPa with

Received: December 27, 2010
Revised: March 13, 2011
Published: May 04, 2011

boron nitride,[14] 1.2 GPa with NaCl,[14] and 1.9 GPa in methanol−ethanol.[15] Most of the previously published results[14,15] proposed tetragonal high-pressure structural models, except for one suggestion of an orthorhombic phase with no additional structural information.[13] In addition, Paolone et al.[13] reported that the high-pressure distorted phase of bulk $LiMn_2O_4$ can be metastable down to ambient conditions if the sample was cycled to above 10 GPa, similar to the metastability behavior of other spinels, like $ZnMn_2O_4$[16] and $NiMn_2O_4$.[17] The origin of the pressure-induced phase transitions is attributed to the reorientation of Mn^{3+} at the octahedral sites.[15]

To elucidate the effect of pressure on the behavior of $LiMn_2O_4$, we investigated the structural transformation and mechanical properties of commercial $LiMn_2O_4$ powder as well as well-characterized $LiMn_2O_4$ nanorods at high pressure using in situ angle dispersive XRD. We found that $LiMn_2O_4$ is extremely sensitive to the nonhydrostatic conditions that result in a pressure-induced phase transition from a cubic phase to distorted tetragonal phases, and the degree of deviatoric stress affects the materials' metastability behavior. A comparison of the morphology difference between the bulk and nanorod samples recovered from hydrostatic pressure conditions indicates that $LiMn_2O_4$ in the nanorod form can accommodate more stress and strain compared to its bulk counterpart. Our results elucidate the origin of this phase transition and demonstrate that pressure studies can provide valuable insight into improving battery technology.

EXPERIMENTAL METHODS

$LiMn_2O_4$ Nanorods Synthesis. The synthesis of $LiMn_2O_4$ nanorods is a two-step approach as shown in previous work.[18,19] First, β-MnO_2 nanorods were synthesized as a template by hydrothermal methods. Typically 8 mmol of $MnSO_4 \cdot H_2O$ and 8 mmol of $(NH_4)_2S_2O_8$ were dissolved in 10 mL of deionized water separately to form clear solutions. They were mixed together and transferred to a 45 mL Teflon-lined stainless steel vessel (Parr Co.). The vessel was sealed and heated at 150 °C for 12 h to obtain β-MnO_2 nanorods. After this step, as-synthesized MnO_2 nanorods were mixed and ground with lithium precursor with a molar ratio of 2:1. One milliliter of methanol was added to make a uniform slurry mixture. After drying, the mixture was sintered at 700 °C for 10 h under air. The nanorods have an average diameter of 100−150 nm and an average length of 1−2 μm. The geometry of the nanostructured materials was observed on a field emission SEM (FE-SEM Philips XL30 FEG, Eindhoven, Netherlands). Transmission electron microscope images and diffraction patterns showed that nanorods are single crystalline and grow along the ⟨110⟩ crystallographic direction.[18,19]

High-Pressure X-ray Diffraction Measurements. Symmetric diamond anvil cells with 500 μm diamond culets were used for the high-pressure measurements. To generate nonhydrostatic conditions, the commercial bulk or nanorod $LiMn_2O_4$, together with a ruby chip for pressure calibration[20] were loaded into the sample chamber created by drilling a hole in a preindented stainless steel gasket. In separate experiments to create a hydrostatic pressure environment, a mixture of methanol−ethanol (4:1) was loaded as a pressure transmitting medium.

In situ high-pressure angle dispersive XRD experiments were performed at beamline 16ID-B of the Advanced Photon Source (APS), Argonne National Laboratory (ANL) and beamline 12.2.2 of the Advanced Light Source (ALS), Lawrence Berkeley National Laboratory (LBL). Diffraction images were collected at a wavelength of λ = 0.4074 Å (APS) and 0.4959 Å (ALS). All the experiments were carried out at ambient temperature. The 2D Debye−Scherrer rings were integrated using the software package *FIT2D*,[21] and *Jade 5* was used to index the diffraction patterns and refine the lattice parameters.[22]

EXPERIMENTAL RESULTS

1. Commercial $LiMn_2O_4$ Powders under Hydrostatic and Nonhydrostatic Conditions. The pristine commercial powders ($LiMn_2O_4$ electrochemical grade, Sigma Aldrich) with a spinel structure of a_0 = 8.2466(6) Å loaded with a mixture of methanol−ethanol underwent a structural change at pressures above 11.0 GPa. Figure 1 shows the development of the X-ray diffraction patterns for commercial $LiMn_2O_4$ powders as a function of pressure up to 15.4 GPa. Above 11.0 GPa, we found evidence for a phase transition, as can be seen by the continuous splitting of the (311), (400), and (511) reflections in the spinel phase into at least three peaks above the transition pressure, indicating coexistence of tetragonal phases ($F4_1/ddm$) with $c/a < 1$ and with $c/a > 1$. $F4_1/ddm$, a straightforward illustration of the tetragonally distorted spinel structure, is an alternative description of the $I4_1/amd$ space group (space group no. 141). The evolution of lattice parameters and volume per molecule of the spinel and tetragonal phases is illustrated in Figure 2. The tetragonal phases showed a similar decrease in molecular volume with pressure, and an increasing or decreasing c/a ratio for the tetragonal $c/a > 1$ or $c/a < 1$ phase respectively. A fit to the third order Birch−Murnaghan (3OBM) equation of state (EOS) up to 11.0 GPa gave a bulk

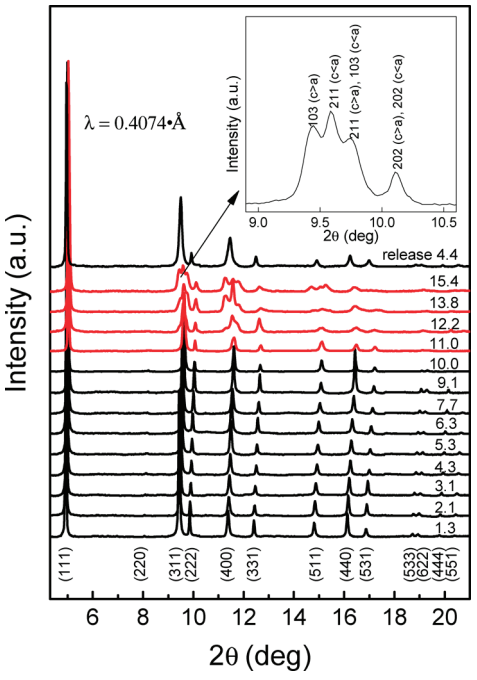

Figure 1. Evolution of the X-ray diffraction patterns of commercial $LiMn_2O_4$ powder in a mixture of methanol−ethanol as a function of pressure up to 15.4 GPa as well as representative decompression pattern. Systematic shifts toward higher 2θ (smaller d-spacing) were observed at pressures below 11.0 GPa due to the compression of the cubic lattice. The phase transition was apparent at 12.2 GPa. The numbers on the right side indicate pressure in GPa. Miller indices for the spinel phase are given at the bottom. The insert shows the reflections of tetragonal $c > a$ and $c < a$ phases at 15.4 GPa in the representative 2θ region.

dx.doi.org/10.1021/jp112289h |J. Phys. Chem. C 2011, 115, 9844–9849

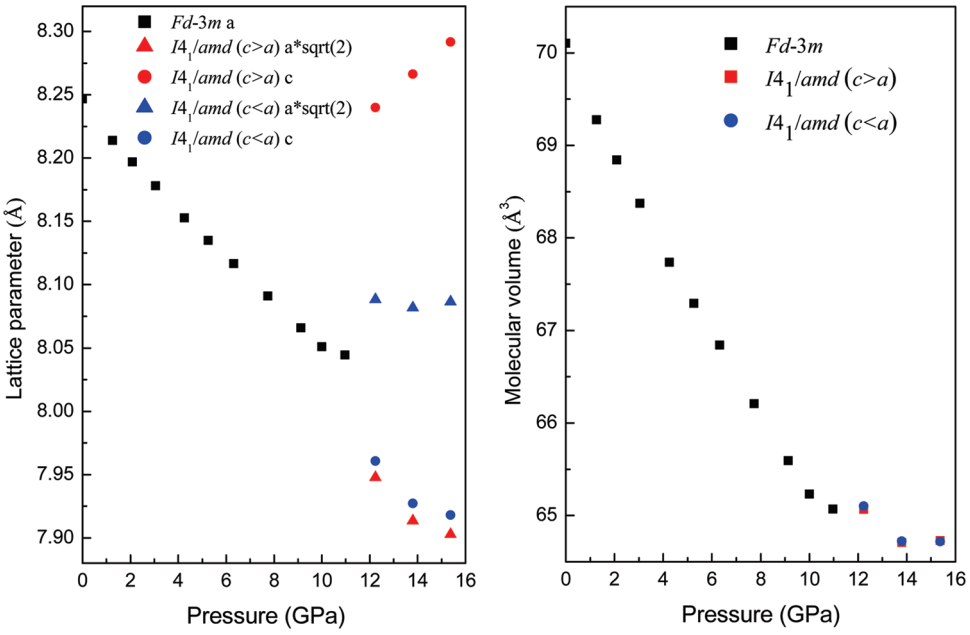

Figure 2. Development of lattice parameters and volume per molecule in the spinel structure and the distorted tetragonal phases of bulk $LiMn_2O_4$ as a function of pressure. The a*sqrt(2) is used in tetragonal phases for straightforward comparison between the undistorted and distorted cubic structures.

modulus K_0 for the spinel $LiMn_2O_4$ bulk of 119(4) GPa. The change in molecular volume and lattice parameters with pressure suggests that the cubic phase continuously distorts into tetragonal $I4_1/amd$ and that the structural transformation is displacive and second-order. The transition was found to be reversible upon releasing the pressure, as the materials transformed back to the original cubic phase.

Under nonhydrostatic conditions, at the starting pressure of 0.4 GPa, the bulk $LiMn_2O_4$ powder had already undergone an irreversible structural transformation to the mixture of distorted tetragonal phases. The structure remained tetragonal as the pressure was increased to 5.3 GPa, as well as after decompression back to ambient pressure. Representative XRD patterns are shown in Figure 3.

SEM analysis was performed to examine whether the morphology of the materials was maintained after the high-pressure experiments. The SEM images clearly showed that the particles after compression in methanol−ethanol remain an intact shape (parts a and b of Figure 4), whereas in contrast the particles became clustered when recovered back from compression under nonhydrostatic conditions (part c of Figure 4).

2. Well-Characterized Synthetic $LiMn_2O_4$ Nanorods under Hydrostatic and Nonhydrostatic Conditions. The measurements on bulk materials clearly indicate that commercial $LiMn_2O_4$ powders display an extremely sensitive structural response to the onset of deviatoric stress under external applied pressure. However, the size of the bulk particles is very heterogeneous (part a of Figure 4). To confirm that the pressure effect we observed is not due to varying grain size, well-characterized synthetic $LiMn_2O_4$ nanorods with an average diameter of 100−150 nm and an average length of 1−2 μm were further investigated under the same experimental conditions as the bulk materials.

The starting $LiMn_2O_4$ nanorods showed a pure *Fd*-3*m* spinel structure with a_0 = 8.2511(2) Å in agreement with the JCPS card No. 35−0782 value (a_0 = 8.24762(16) Å).[22] The compressional behavior of $LiMn_2O_4$ nanorods loaded with a mixture of

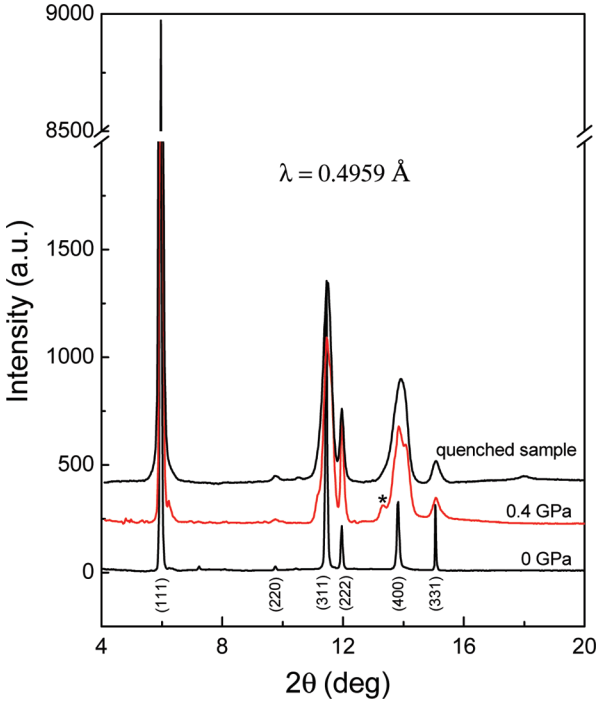

Figure 3. X-ray diffraction patterns for commercial $LiMn_2O_4$ powder in a diamond anvil cell under nonhydrostatic conditions from bottom to top: at 0 GPa before compression, 0.4 GPa, and for the quenched sample after releasing the pressure. The asterisk represents the peak from the stainless steel gasket. Miller indices for the spinel phase are given at the bottom.

methanol−ethanol was investigated up to 17.2 GPa and a similar reversible phase transition was observed at pressures above 10.5 GPa (Figure 5). The development of lattice parameters and molecular volume of the spinel and the tetragonal phases

dx.doi.org/10.1021/jp112289h |*J. Phys. Chem. C* 2011, 115, 9844–9849

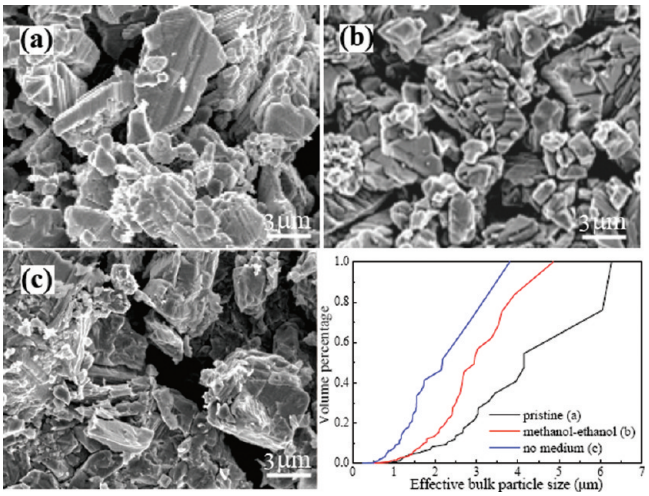

Figure 4. SEM images of (a) pristine commercial $LiMn_2O_4$ powder, (b) bulk samples after compression in a mixture of methanol−ethanol, and (c) the quenched bulk samples after compression without pressure medium. Statistical analysis of images (a)−(c) shows the accumulation of volume percentage as a function of the particle size.

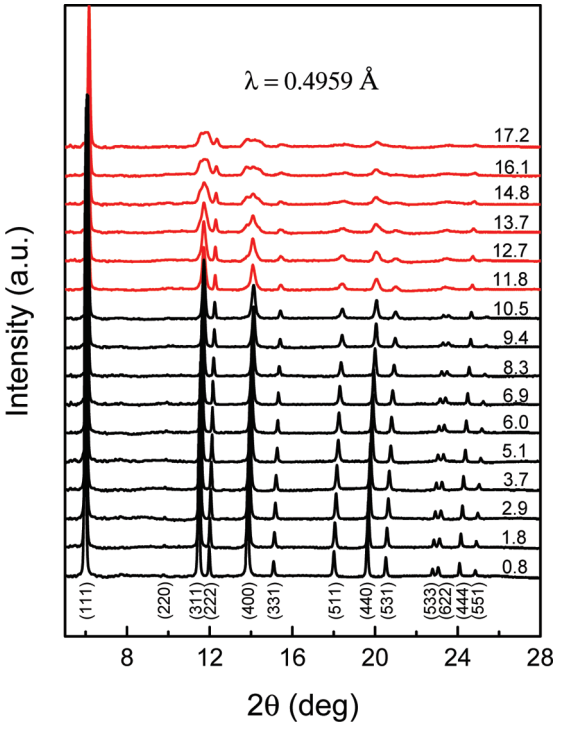

Figure 5. Evolution of X-ray diffraction patterns of $LiMn_2O_4$ nanorods as a function of pressure up to 17.2 GPa at ambient temperature. Systematic shifts toward higher 2θ were observed at pressures below 10.5 GPa due to the compression of the cubic lattice. The phase transition was apparent at 11.8 GPa. The numbers on the right side indicate pressure in GPa. Miller indices for the spinel phase are given at the bottom.

with pressure is shown in Figure 6. A fit of the 3OBM EOS up to 10.5 GPa gave a bulk modulus K_0 for the spinel $LiMn_2O_4$ nanorods of 119(1) GPa. In contrast, the $LiMn_2O_4$ nanorods had already undergone an irreversible structural change at the initial pressure point of 0.7 GPa under nonhydrostatic conditions. SEM analysis on the quenched nanorods showed a contrast in morphologies resulting from hydrostatic versus nonhydrostatic conditions (Figure 7). The reversibility or irreversibility of the transition was also tied to the observed preservation or loss of the original nanorod morphology.

In addition, the nanorods were examined using helium as the pressure transmitting medium. However, the sample was precompressed between two anvils before loading into the gasket hole where some extent of nonuniform external deviatoric stress was exerted. Interestingly, after gas loading was performed where the sample was sealed at 1.3 GPa, we found that the sample was mostly transformed into the distorted structure but there was an area with the original spinel structure. As pressure was increased to the highest 18.2 GPa where helium still provides good hydrostaticity,[23] this area still remained in the cubic structure and did not transform to the mixture of tetragonal phases.

DISCUSSIONS

Our studies of the effect of pressure on $LiMn_2O_4$ commercial powders and well-characterized nanorods under hydrostatic and nonhydrostatic conditions indicate that $LiMn_2O_4$ is extremely sensitive to deviatoric stress induced by external applied pressure. The transition pressure for $LiMn_2O_4$ in methanol−ethanol occurred around 11 GPa, which coincides with where the pressure medium reaches its hydrostatic limit,[24] whereas the samples without pressure medium transformed immediately when the external pressure was applied. However, all previous studies on bulk $LiMn_2O_4$ reported that a pressure-induced structural transition occurs at quite low pressures below 2 GPa with different pressure media giving rise to slightly different transition pressures, with the highest transition pressure reported to be 1.9 GPa in methanol−ethanol.[13−15] This disparity might result from differing starting materials due to synthesis methods but our results indicate that this discrepancy is more likely related to the quality of the pressure medium. Another possible explanation for the disagreement is that in previous studies samples may be bridging between the anvils that would result in nonhydrostatic conditions even in methanol−ethanol.

The degree of deviatoric stress also affects the metastability of the quenched materials. Although the highest pressures reached with methanol−ethanol in both bulk and nanorod $LiMn_2O_4$ (>15 GPa) were much higher than those under nonhydrostatic conditions (~5 GPa), the phase transition was reversible in methanol−ethanol, whereas in contrast the high-pressure phase could be recovered back to ambient pressure when no pressure medium was used. This result indicates that deviatoric stress rather than absolute pressure is the key component for quenching the high-pressure phase and further confirms the role that deviatoric stress plays in this phase transition. In addition, SEM images capture how the morphology of the samples is modified under compression. Statistical analysis on the dimensions of the recovered samples shows that particles in both bulk and nanorod form underwent different magnitude of shrinkage after compression (part d of Figure 4 and part d of Figure 7). In particular, under nonhydrostatic conditions, samples' morphology is completely destroyed and the particles crack to a much greater extent, especially the nanorods. Part d of Figure 7 unambiguously reveals that nanorods recovered from hydrostatic versus nonhydrostatic conditions experienced a very small shrinkage versus a huge reduction of the nanorod length respectively. In both cases, the nanorod diameter was maintained. This suggests that spinel $LiMn_2O_4$ has a limited tolerance to deviatoric stress, above which it undergoes an irreversible phase transition.

dx.doi.org/10.1021/jp112289h |J. Phys. Chem. C 2011, 115, 9844–9849

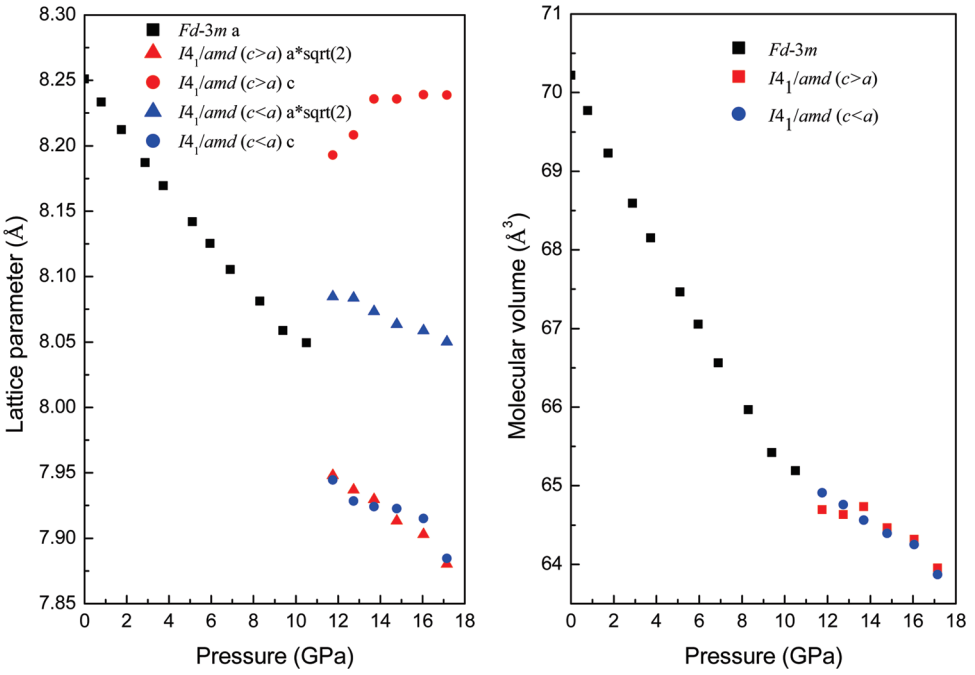

Figure 6. Development of lattice parameters and volume per molecule in the spinel structure and the distorted tetragonal phases in $LiMn_2O_4$ nanorods as a function of pressure. The a*sqrt(2) is used in tetragonal phases for straightforward comparison between the undistorted and distorted cubic structures.

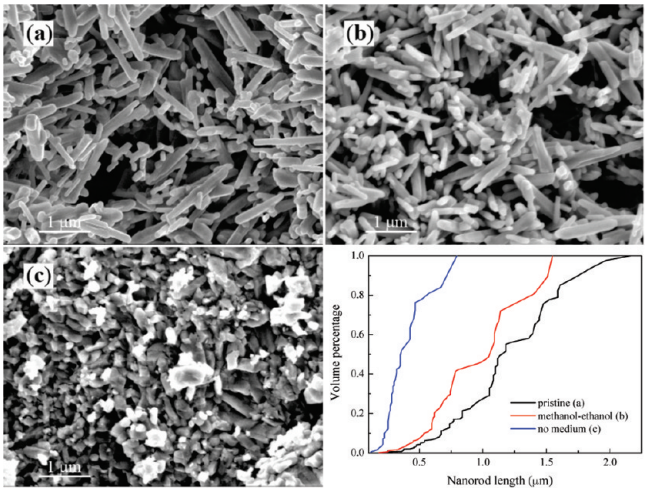

Figure 7. SEM images of (a) well-characterized pristine $LiMn_2O_4$ nanorods before compression, (b) quenched nanorods after compression in a mixture of methanol−ethanol, and (c) after compression without pressure medium. Statistical analysis of images (a)−(c) showing the accumulation of volume percentage as a function of nanorod length quantifies the significant morphology change between the nanorods under nonhydrostatic conditions and the pristine nanorods as well as those quenched from hydrostatic compression.

We further notice that the nanorod samples show smaller particle size reduction compared to their bulk counterparts after compression in methanol−ethanol, although the highest pressure reached in bulk sample of 15.4 GPa was lower than that in nanorods of 17.2 GPa (part b of Figure 4 vs part b of Figure 7). This observation indicates that the nanorods can accommodate more stress and strain before they reach the critical limit, consistent with the conclusion in recent work predicting that the critical power rate for fracture decreases with increasing particle size.[10] Our result is also in agreement with high-pressure studies on other nanocrystalline materials, which indicate that they often exhibit enhanced mechanical properties compared with their bulk counterparts.[25−28]

Because of the presence of multiple phases including the tetragonal $c/a > 1$, tetragonal $c/a < 1$, and the cubic structure at high pressure, as well as peak broadening caused by the nonhydrostatic conditions, it is not reliable to fully separate the reflections belonging to each phase and quantitatively determine their relative abundance, especially the tetragonal $c/a < 1$ and the cubic phases owning to the overlapping of the main (211) reflection in the tetragonal $c/a < 1$ and the cubic (311). However, the (103) reflection in the tetragonal $c/a > 1$ phase is well separated (insert in Figure 1) and becomes increasingly intense with pressure, indicating the growth of the tetragonally elongated structure under compression at the expense of the other two phases. This observation along with the increased c/a ratio in tetragonal $c > a$ phase in both bulk and nanorods reveals that pressure tends to orient the distorted $Mn^{3+}O_6$ octahedra in a fashion that the elongated direction is parallel to the c axis, which enables the expression of the Jahn−Teller distortion. This structural evolution from a Jahn−Teller inactive phase to an active one is opposite to what has been observed in other manganites at high pressure where the Jahn−Teller distortion is usually reduced due to the delocalization of electrons, the change in spin configuration, or the charge disproportionation that occurs with compression.[29−32] It is expected that at higher pressures the Jahn−Teller distortion would eventually be suppressed although $LiMn_2O_4$ may also undergo other phase transitions before this occurs. The correlation between the manifestation of the Jahn−Teller distortion and deviatoric stress also suggests that $LiMn_2O_4$ may have a higher tolerance to excess lithium, which could extend its 3 V plateau for practical use with modest hydrostatic external pressure.

dx.doi.org/10.1021/jp112289h |J. Phys. Chem. C 2011, 115, 9844–9849

Previous experimental studies indicate that oxide spinels with the same cation oxidation states have similar bulk moduli around 200 GPa.[16,17,33−35] This was theoretically explained as being related to the oxidation state of the cation accommodated in the interstitial sites of the face-centered cubic array of oxygen anions, which is responsible for the cation polyhedral compressibility and controls the bulk modulus.[36] The lower the oxidation state of the cation, the larger the size of the polyhedra, which leads to a weaker cation−oxygen bond, and a higher compressibility. Therefore, lithium−manganese oxides ($Li_xMn_{3-x}O_4$) exhibit greatly enhanced compressibilities compared with other types of oxide spinels. In our study, fits of the 3OBM EOS to the experimental $LiMn_2O_4$ commercial powder and nanorod data gave a similar value of the bulk modulus as low as 119 GPa. Their high compressibilities among oxide spinels may be correlated with their sensitivity to deviatoric stress.

CONCLUSIONS

The effect of pressure on the structure of $LiMn_2O_4$ commercial powders and well-characterized nanorods was examined by in situ X-ray diffraction at high pressure under conditions of varying hydrostaticity. The observation that bulk materials underwent a structural transformation under nonhydrostatic compression at much lower pressure compared to hydrostatic compression indicates that stoichiometric $LiMn_2O_4$ is extremely sensitive to deviatoric stress. The comparative study of well-characterized $LiMn_2O_4$ nanorods underscores the role of deviatoric stress in triggering the phase transition driven by the Jahn−Teller distortion due to the reorientation of $Mn^{3+}O_6$ octahedra. The metastability field of the high-pressure phase was greatly influenced by the degree of deviatoric stress. The observation that the nanorod samples can accommodate more stress and strain than the bulk material indicates that nanostructured materials can enhance their mechanical property for better battery performance. Our high-pressure studies improve our understanding of this material's fundamental physical and chemical properties and provide guidance for developing approaches of synthesizing improved battery materials.

AUTHOR INFORMATION

Corresponding Author

*E-mail: lyforest@stanford.edu.

ACKNOWLEDGMENT

This work was supported by the Department of Energy (DOE) under Award Number DE-FG02-07ER46461, the Stanford Institute for Materials & Energy Science DE-AC02-76SF00515. The experiments were performed at ALS beamline 12.2.2, LBL, and HPCAT (Sector 16), APS, ANL. HPCAT is supported by DOE-BES, DOENNSA, NSF, and the W.M. Keck Foundation. APS is supported by DOE-BES, under Contract No. DE-AC02-06CH11357. We also thank S. Sinogeikin, Y. Ding, Y. Meng, M. Baldini, S. Wang, and D. Lin for assistance with the XRD experiments and data interpretation, and EFree for travel support. Y. Lin and Y. Yang acknowledge support from Stanford Graduate Fellowships.

REFERENCES

(1) Scrosati, B. *Nature* **1995**, *373*, 557–558.
(2) Chung, S. Y.; Bloking, J. T.; Chiang, Y. M. *Nat. Mater.* **2002**, *1*, 123–128.
(3) Whittingham, M. S. *Chem. Rev.* **2004**, *104*, 4271–4301.
(4) Kang, K. S.; Meng, Y. S.; Breger, J.; Grey, C. P.; Ceder, G. *Science* **2006**, *311*, 977–980.
(5) Manthiram, A.; Vadivel Murugan, A.; Sarkar, A.; Muraliganth, T. *Eng. Environ. Sci.* **2008**, *1*, 621–638.
(6) Jayalakshmi, M.; Rao, M. M.; Scholz, F. *Langmuir* **2003**, *19*, 8403–8408.
(7) Cabana, J.; Valdes-Solis, T.; Palacin, M. R.; Oro-Sole, J.; Fuertes, A.; Marban, G.; Fuertes, A. B. *J. Power. Sources* **2007**, *166*, 492–498.
(8) Luo, J. Y.; Wang, Y. G.; Xiong, H. M.; Xia, Y. Y. *Chem. Mater.* **2007**, *19*, 4791–4795.
(9) Tarascon, J. M.; Wang, E.; Shokoohi, F. K.; Mckinnon, W. R.; Colson, S. *J. Electrochem. Soc.* **1991**, *138*, 2859–2864.
(10) Woodford, W. H.; Chiang, Y.-M.; Carter, W. C. *J. Electrochem. Soc.* **2010**, *157*, A1052–A1059.
(11) Yamada, A.; Tanaka, M. *Mater. Res. Bull.* **1995**, *30*, 715–721.
(12) Rodriguez-Carvajal, J.; Rousse, G.; Masquelier, C.; Hervieu, M. *Phys. Rev. Lett.* **1998**, *81*, 4660–4663.
(13) Paolone, A.; Sacchetti, A.; Postorino, P.; Cantelli, R.; Congeduti, A.; Rousse, G.; Masquelier, C. *Solid State Ionics* **2005**, *176*, 635–639.
(14) Piszora, P. *Z. Kristallogr. Suppl.* **2007**, *26*, 387–392.
(15) Piszora, P.; Nowicki, W.; Darul, J.; Bojanowski, B.; Carlson, S.; Cerenius, Y. *Radiat. Phys. Chem.* **2009**, *78*, S89–S92.
(16) Asbrink, S.; Waskowska, A.; Gerward, L.; Olsen, J. S.; Talik, E. *Phys. Rev. B* **1999**, *60*, 12651–12656.
(17) Asbrink, S.; Waskowska, A.; Olsen, J. S.; Gerward, L. *Phys. Rev. B* **1998**, *57*, 4972–4974.
(18) Kim, D. K.; Muralidharan, P.; Lee, H. W.; Ruffo, R.; Yang, Y.; Chan, C. K.; Peng, H.; Huggins, R. A.; Cui, Y. *Nano Lett.* **2008**, *8*, 3948–3952.
(19) Yang, Y.; Xie, C.; Ruffo, R.; Peng, H. L.; Kim, D. K.; Cui, Y. *Nano Lett.* **2009**, *9*, 4109–4114.
(20) Mao, H. K.; Xu, J.; Bell, P. M. *J. Geophys. Res.* **1986**, *91*, 4673–4676.
(21) Hammersley, A. P.; Svensson, S. O.; Hanfland, M.; Fitch, A. N.; Hausermann, D. *High Pressure Res.* **1996**, *14*, 235–248.
(22) *Jade 5.0*, Materials Data Inc.: Livermore, CA, USA, 1998.
(23) Takemura, K. *J. Appl. Phys.* **2001**, *89*, 662–668.
(24) Angel, R. J.; Bujak, M.; Zhao, J.; Gatta, G. D.; Jacobsen, S. D. *J. Appl. Crystallogr.* **2007**, *40*, 26–32.
(25) Wang, Z. W.; Saxena, S. K.; Pischedda, V.; Liermann, H. P.; Zha, C. S. *Phys. Rev. B* **2001**, *64*, 012102.
(26) Zhang, J. Z.; Zhao, Y. S.; Palosz, B. *Appl. Phys. Lett.* **2007**, *90*, 043112.
(27) Guo, Q. X.; Zhao, Y. S.; Mao, W. L.; Wang, Z. W.; Xiong, Y. J.; Xia, Y. N. *Nano Lett.* **2008**, *8*, 972–975.
(28) Wang, L.; Liu, B. B.; Liu, D. D.; Yao, M. G.; Yu, S. D.; Hou, Y. Y.; Zou, B.; Cui, T.; Zou, G. T.; Sundqvist, B.; Luo, Z. J.; Li, H.; Li, Y. C.; Liu, J.; Chen, S. J.; Wang, G. R.; Liu, Y. C. *Appl. Phys. Lett.* **2007**, *91*, 103112.
(29) Congeduti, A.; Postorino, P.; Caramagno, E.; Nardone, M.; Kumar, A.; Sarma, D. D. *Phys. Rev. Lett.* **2001**, *86*, 1251.
(30) Baldini, M.; Di Castro, D.; Cestelli-Guidi, M.; Garcia, J.; Postorino, P. *Phys. Rev. B* **2009**, *80*, 045123.
(31) Loa, I.; Adler, P.; Grzechnik, A.; Syassen, K.; Schwarz, U.; Hanfland, M.; Rozenberg, G. K.; Gorodetsky, P.; Pasternak, M. P. *Phys. Rev. Lett.* **2001**, *87*, 125501.
(32) Santillán, J.; Shim, S. H.; Shen, G. Y. Prakapenka, V. B. *Geophys. Res. Lett.* **2006**, *33*, doi:10.1029/2006GL026423.
(33) Kruger, M. B.; Nguyen, J. H.; Caldwell, W.; Jeanloz, R. *Phys. Rev. B* **1997**, *56*, 1–4.
(34) Waskowska, A.; Gerward, L.; Olsen, J. S.; Steenstrup, S.; Talik, E. *J. Phys. Condens. Mat.* **2001**, *13*, 2549–2562.
(35) Gerward, L.; Jiang, J. Z.; Olsen, J. S.; Recio, J. M.; Waskowska, A. *J. Alloys Compd.* **2005**, *401*, 11–17.
(36) Recio, J. M.; Franco, R.; Pendas, A. M.; Blanco, M. A.; Pueyo, L. *Phys. Rev. B* **2001**, *63*, 7.